Delft University of Technology

Comparative Performance of Inverted-Based Generation using Synchonverter during Transient Stability Conditions

Gonzalez-Longatt, Francisco; Rueda, Jose Luis; Palensky, Peter; Chamorro, Harold R.; Abdellah, Kouzou

Citation (APA)
Gonzalez-Longatt, F., Rueda, J. L., Palensky, P., Chamorro, H. R., & Abdellah, K. (2022). Comparative Performance of Inverted-Based Generation using Synchonverter during Transient Stability Conditions. In *Proceedings - 2022 5th International Conference on Power Electronics and their Applications, ICPEA 2022* (Proceedings - 2022 5th International Conference on Power Electronics and their Applications, ICPEA 2022). IEEE. https://doi.org/10.1109/ICPEA51060.2022.9791140

Important note
To cite this publication, please use the final published version (if applicable).
Please check the document version above.

Comparative Performance of Inverted-Based Generation using Synchonverter during Transient Stability Conditions

Francisco Gonzalez-Longatt
Department of Electrical Engineering,
Information Technology and Cybernetics
University of South Eastern Norway
Porsgrunn, Norway
fglongatt@fglongatt.org

Jose Luis Rueda and Peter Palensky
Department of Electrical Sustainable
Energy
Delft University of Technology
Delft, Netherlands
{J.L.RuedaTorres,
P.Palensky}@tudelft.nl

Harold R. Chamorro
Department of Electrical Sustainable
Energy
KTH, Royal Institute of Technology
Stockholm, Sweden
hrcv@kth.se

Kouzou Abdellah
Laboratoire d'Automatique appliquéé et
Diagnostics Industriel (LAAD)
Université de Djelfa
Djelfa, Algeria
a.kouzou@univ-djelfa.dz

Abstract—**Inverter-based generation (IBG) is critical in achieving a dependable and resilient electrical system while meeting the net-zero emission goal. The enormous integration of IBG tends to produce various issues, including reduced rotational inertia and reduced short circuit levels. Several scientific publications agree that the voltage source converters (VSCs) empowered by the so-called grid forming (GFM) control may provide a lasting answer for reaching the future net-zero IBG-dominated power systems. This paper presents a comparative analysis of the dynamic performance between IBR using synchronverter and a traditional synchronous generator (SG), where the specific concern is the transient stability conditions. DIgSILENT PowerFactory has been used for time-domain simulations using a test system, and numerical simulations considering an N-1 event prove the significant benefit of GFN converter controls in providing active power during a voltage sag induced by a short circuit condition, allowing the system to endure longer short circuit durations.**

Keywords—power electronic converter, contingency, grid-forming, grid-following, transient stability, short circuit.

I. INTRODUCTION

Current power networks are undergoing substantial transformation, which is tied to all aspects of the electrical sector [1], [2], [3]: (i) generation-side: deployment and use of more environmentally friendly and weather dependent technologies [4], (ii) grid-side: integration of more flexible assets where the use of direct current (DC) and other technologies (FACTS and storage) are vital elements [5], (iii) demand-side: the rise of novel technologies behind the meter such as small-scale battery energy storage (BESS), electric cars, and the huge transformation of the costumer evolving for a very passive role and the emergence of the concept of the prosumer, prosumers concept is a reality in various nations across the world [6], [7]. The aforementioned power system transformation shares numerous characteristics, but the unifying denominator is the massive integration of IBG [8], [9]. The IBG is a vital component in achieving a reliable and sustainable energy transition, as it is a component of the vast integration of the so-called "low-carbon technologies". Those technologies use the power electronic converter (PEC) as the crucial interface between the generation/storage technology and the power grid [6], [10].

Many academics attempted to answer a broad question: what is the problem caused by the extensive integration of power converters? In reality, this subject is general and may be interpreted in various ways; it is undeniably true that the increasing penetration of IBG displaces the number of synchronous generators (SGs) accessible in the power system. As a result, this study topic must be carefully addressed from two perspectives: those generated by the IBG itself (intrinsically related to the quick and complicated dynamics of the PEC control loops), and those induced by limiting the number of SGs connected to the power network. The scientific community has intensively examined these challenges, with several recent research publications and initiatives identifying two critical concerns [11], [12]: (i) Low (to none) supply of total system rotational inertia and (ii) Reduced and limited fault levels affecting short circuit ratio (SCR). Several institutions/organisations have highlighted and acknowledged the concerns associated with the widespread use of IBG and the lowering of SGs, e.g., system operators, academia, and manufacturers [13]. Moreover, several sources highlight recurring themes linked with the IBG's characteristic traits. [14]: (i) The lack of robustness (especially during extremely high overcurrent events and massive voltage drops), (ii) Failure of the Phase-locked loop (PLL) to follow very deep voltage

sags [15], (iii) Fault ride-through (FRT) failures, and (iv) Adverse interactions.

The IEEE Power System Dynamic Performance Committee recognised the necessity to include new kinds of electrical power system dynamic behaviour with significant penetration of power electronic interfaced technology in April 2020 [16]; as a result of the penetration of PEC-interfaced technologies into bulk power systems, the categorisation and definition of power system stability phenomena were increased. Consequently, two new stability classes were created [16]: Converter-driven stability and resonance stability.

From the dynamic behaviour point of view, the PEC-based technologies or the IBG are significantly different from the transitional SGs, those differences are several, but the main reason for them re attributable to the nature of the voltage-source converter (VSC) interface with the power grid and the related control loops [16]. It has been documented in several scientific publications that the IBG has a peculiar dynamic behaviour during some system conditions, and the specific dynamic can produce oscillations that create local instabilities in the power network; this king of behaviour is named converter-driven instabilities [16]. In most cases, the instability phenomenon is the consequence of erroneous controller settings or controllers that are poorly constructed. However, replacing traditional SGs with IBGs is a double-edged sword; poor control settings might produce instability issues, but if suitable control loops are activated with appropriate settings, IBGs give a solution to many power system difficulties such as low rotational inertia [14]. Furthermore, PEC-interfaced technologies that replace traditional SGs might be equipped with control loops to respond swiftly to any contingency. One important fact of the IBG technologies is that they can react far quicker than the very slow electromechanical dynamic exhibited by the SGs [14]. When suggesting solutions to difficulties connected to the IBG-dominated power system, there are two pathways to consider: short-term and long-term solutions. It has been recognised that one of the very positive long-term options is to use GFM control as a technique to enable the VSC with some of the forming characteristics of the traditional SGs.

The GFM control strategy of PECs, from a systemic point of view, isa very important research topic of the authors of this paper. The researchers in this paper have already published a quick look at the dynamic performance of the GFR control technique of VSC during short-circuit [14].

In this research paper, the authors present a comparative analysis (when possible, between inverted based generation using synchonverter and a traditional SG during transient stability events. A very simple test system is used by the authors in this scientific paper; it consists of a generation unit connected to an infinite busbar using a simple transmission system. For simulation purposes, the test system and the GFM models have been implemented in DIgSILENT PowerFactory. Section II presents the key features for modelling and simulation of VSC control techniques. Section III presents a very short introduction to the SG emulation control and presents details of the three GFM controllers realised in this scientific paper. The numerical results of the experiments and

the analysis emerging time-domian response of the different technologies are shown un Section IV. Lastly, the most important conclusions and findings in this scientific paper are presented in Section V.

II. VSC CONTROL TECHNIQUE

Grid-connected VSC-based PECs offer a very flexible interface between the primary energy source/storage and the power network. (see Fig. 1) [14]. Traditionally the control techniques applied to the VSC can be grouped into (i) Grid-forming (GFM) control and (ii) Grid-following (GFL). An ideal current source (I_{ref}) connected to the grid in parallel with high impedance (Z) is used to represent the GFL converters, typically [14], [17] -details in Fig. 2.a. The GFM control enables a VSC with functionalities that enable the converter to replicate (in some sense) the SG and support the power network operation [14]. The GFM normally is modelled as a controlled voltage source that is controlled in order to provide an adequate controller voltage (V_{ac}) and frequency (f) to the power network (mode details in Fig. 2.b and Fig. 4).
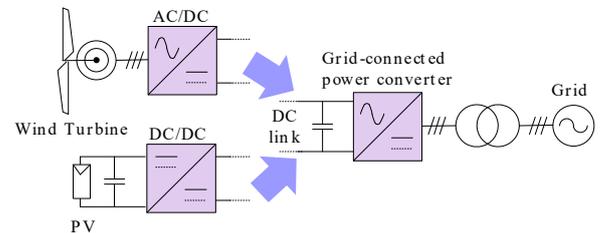
Fig. 1. Illustration of the use of PEC to integrate PV and wind power generation into the power network [14].

(a) Simplified model of GFL technique applied to a current source model.

(b) Simplified model VSC with GFM control.
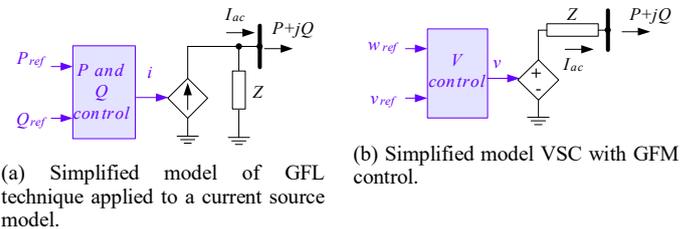
Fig. 2. Simplified model of (a) GFL and (b) GFM implementations.

III. GRID FORMING CONTROLLER: SYNCHRONVERTER

The GFR control technique for VSC is a method for using the IBG as a controlled voltage source in series with an impedance. The power electronic converter (PEC) may mimic the behaviour of synchronous generators using this circuit-based technique (inside the inherent differences between a PEC and SG). Fig. 3 depicts a non-exhaustive review of the key control strategies used to simulate the behaviour of a synchronous generator. More information and a linked description of those control measures are available at [18]. In this scientific paper, the GFM control and PEC consist of a VSC and the control. The PEC is modelled as a controllable AC voltage source in series with a series output impedance (Z_{vi}) -see Fig. 4 for more details. The so-called virtual impedance (Z_{vi}) is modelled considering the dq-axis reference system as Z_{vi}

$= r_{vi} + jx_{vi}$. The d-axis and q-axis voltage drop over an algebraic type of virtual impedance are calculated as follows [14]:

$$\Delta v_{vi,d} = r_{vi}i_d - x_{vi}i_q$$
$$\Delta v_{vi,q} = r_{vi}i_q + x_{vi}i_d \qquad (1)$$
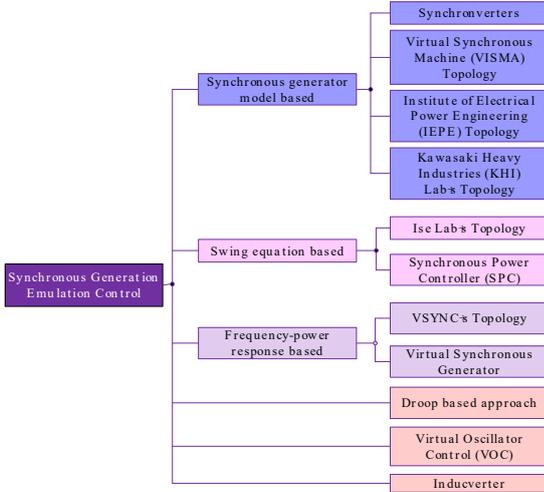
Fig. 3. General overview of the control techniques used for the implementation of GM emulation (no exhaustive) using PEC [14].
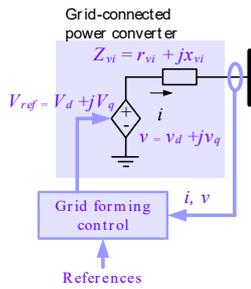
Fig. 4. GFR converter with virtual inertia (VI) concept.

The pioneering idea behind the Synchronverter control technique (SynC) was initially presented by Q. Zhong and G. Weiss in a scientific paper titled "*Synchronverters: Inverters that mimic synchronous generators*" in 2011 [19]. In this paper, the author decided to use the SynC technique presented in [19]. The application of the electromechanics dynamic is the fundamental distinction between the SynC and the VSM. The electromechanical dynamic of the machine in the SynC is guided by [14]:

$$\begin{cases} T_{acel}\dfrac{d\theta^2(t)}{dt^2} = T_{ref} - T_{actual} - D_p\dfrac{d\theta(t)}{dt} \\ \dfrac{d\theta(t)}{dt} = \left(\omega_r - \omega_{ref}\right) \end{cases} \qquad (2)$$

where the electrical toque (T_{actual}) is calculated as:

$$T_{actual} = M_f i_f \sin\theta \qquad (3)$$

in this case, i_f represents the imaginary field (related to the rotor) winding of the SynC fed by an adjustable DC source, and M_f represents the imaginary mutual inductance between the field winding and three winding located at the stator. The voltage of the internal voltage source (v) is calculated as:

$$v = \frac{d\theta}{dt}M_f i_f \sin\theta \qquad (4)$$

The active (p_{calc}) are reactive power (q_{calc}) are defined as:

$$\begin{cases} p_{calc} = \dfrac{d\theta}{dt}M_f i_f i \sin\theta \\ q_{calc} = -\dfrac{d\theta}{dt}M_f i_f i \cos\theta \end{cases} \qquad (5)$$

The injection of the reactive power to the power network can be obtained by using a voltage-droop control; the reactive power error (Δq) is calculated as

$$\Delta q = q_{ref} - q_{calc} - D_q\left(v - v_{ref}\right) \qquad (6)$$

Here, q_{ref} represents the reference of reactive power, q_{calc} signifies the calculated reactive power, v defines the measured voltage, v_{ref} represents the reference voltage, and D_q is the voltage droop coefficient.

IV. EXPERIMENTS

This paper is dedicated to investigating the performance of a single machine connected to an infinite busbar, also known as SMIB, during a fault regime. For experimental objectives, the test system comprises a generation unit connected to a large equivalent power system (assumed as an infinite busbar), a step-up transformer (T_1) and two overhead transmission lines (named Line 1 and Line 2), and a step-down transformer (T_2) (see Fig. 5).
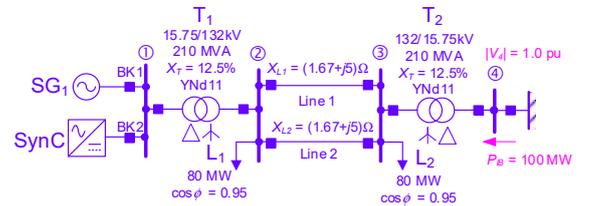
Fig. 5. Single line diagram showing the proposed *Test System*. It consists of a generation technology (SynC or SG activate one at a time) connected to an infinite bus.

Two loads are added, one at the bus ② and the other at ③ and both are modelled as constant power (L1 and L2, respectively). The experiments presented in this section are dedicated to evaluating the performance before the contingency, during and after. A bolted three-phase short circuit is used as the primary contingency in this paper. The short circuit is assumed to occur in the middle of the transmission line "Line 1", and Line 2 remains unaffected transmitting power to the infinite bus.

The performance dynamic of the SMIB is initially assessed considering the machine to be an SG (breaker BK1 closed and BK2 open), and then the SynC is activated and assessed (breaker BK1 open and BK2 closed). The generation unit consists of SG, 210 MVA apparent power, 15.47 kV rated voltage, and fp = 0.8 rated power factor. The SG is modelled

considering the full sixth order dynamic model. The generator model consists of three rotor loops representing the excitation and three damper windings (one on the d-axis and two on the q-axis). The SynC has been modelled as shown in Section III, and Tables I and II present details of the parameters used for each one of the model. It is appropriate to mention that the electromechanical related parameter of the controllers has been updated to be equal to SG.

A. Assessing the critical fault clearing time of synchronous dominated system

A preliminary rotor angle transient stability assessment is performed in the SMIB, considering only synchronous generation. The assessment consists of determining the critical fault clearing time (CFCT). This analysis is performed by using a co-simulation framework based on DIgSILENT PowerFactory, Python API and a Python script. DIgSILENT PowerFactory is used as a power system solution engine, and the interface and script in Python are systematically used to calculate the critical fault creating time. The preliminary assessment of the SMIB considering SG indicates that the CFCT considering a bolted three-phase short circuit is $t_{CFCT} = 0.978$sec. The CFCT is relatively high as the transmission line Line 2 remains transmitting power to the infinite busbar during the fault; this active power flow allows reducing the acceleration power at the SG during the fault condition. Also, it is crucial to notice that the generation unit is equipped with a gas turbine governor that also helps to improve the transient stability of the SMIB.

TABLE I.   SynC CONTROL MODEL: PARAMETERS USED

Meaning	Parameter	Value
Acceleration time	T_{acel}	18.36 sec
Damping coefficient	D_p	100.00pu
Voltage control gain	K_p	1000 pu
Reactive power drop coefficient	D_q	20.00 pu
Damping filter cut-off frequency	ω_r	0.00 rad/sec

TABLE II.   USED IN SynC CONTROL MODEL: PARAMETERS USED

Meaning	Parameters	Value
Virtual resistance	r	0.006 pu
Virtual reactance	x	0.006 pu
Maximum value of allowed overcurrent	I_{lim}	1.01 pu
Proportional factor of additional resistance	k_{pr}	8.00 pu
Proportional factor of additional reactance	k_{px}	8.00 pu
Time constant of low pass filter	T_{lpf}	0.0001 sec

Fig. 6 is used to illustrate the performance of the SMIB system considering stable and unstable conditions. As demonstrated in Fig. 6, the plot of the time series of the rotor angle is presented considering two scenarios: (i) fault is successfully cleared at $t = 0.978$ sec ($<t_{CFCT}$), demonstrating the rotor angle stability of the SMIB system and then, (ii) the fault is cleared at $t = 0.979$ sec ($>t_{CFCT}$), and as observed in Fig. 6, the rotor angle passed 180 electrical degrees or 2π radians which clearly indicates the transient rotor angle instable. Fig. 7 shows the dynamic evolution of the current magnitude ($|I|$) provided by the synchronous generator previous, during and

post short circuit. As expected, the short circuit contribution, immediately after the insertion of the short circuit, reaches several times the rated current ($I_{cc} = 20.76$ kA, $\sim 2.69 \times I_n$ @ $t = 0.0$ sec). The current magnitude decreases as the terminal voltage is reduced by the significant voltage drop caused by the three-phase short circuit at Line 1, the automatic voltage regulator acts, and reactive power experiences a significant increase during the faults period ($Q_{SG1} = -165.4$ MVAR @ $t = 2.32$ sec). When the fault is cleared (stable or not), the current magnitude experiences another peak even higher than the peak created by the short circuit ($I_{cc} = 21.01$ kA, $\sim\sim 2.73 \times I_n$). Finally, the current magnitude reaches the steady-state post contingency current (~16secs ~80 cycles, 2.35 kA). The dynamic response of the SG1 follows the traditional current response provided by an SG.
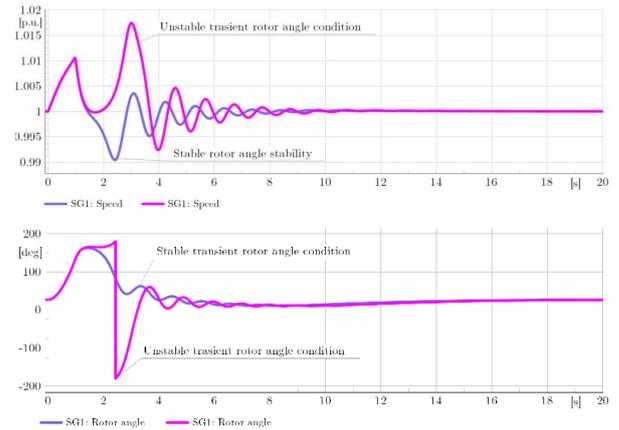
Fig. 6. Plot of rotor angle (θ_r) and speed (ω_r) of SG1 during a transient rotor angle stability. Stable condition when fault is cleared at $t < t_{CFCT} = 0.977$ sec and unstable at $t > t_{CFCT} = 0.979$ sec.
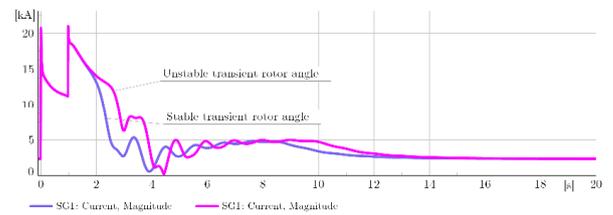
Fig. 7. Plot of current magnitude ($|I|$) of SG$_1$ during a transient rotor angle stability. Stable condition when fault is cleared at $t < t_{CFCT} = 0.977$ sec and unstable at $t > t_{CFCT} = 0.979$ sec.

Fig. 8 shows the trajectories created by the active and reactive power in the PQ-plane. From the steady-state pre-contingency equilibrium point, a reduction in the active power (P) and an increase in the reactive power (Q) is observed to follow the same pattern during the short circuit (both stable and unstable dynamic follow the same line), but then, when the fault is cleared the PQ-trajectory depends on the clearing time, the stable dynamic will produce damped oscillations where the P barely crosses the negative side. Still, the unstable post contingency dynamic exhibits significant exclusions in P, and Q. Fig. 9 shows the locus of the impedance magnitude ($|Z|$ in primary Ohms) measured at the terminal connected to ② of the

faulted transmission line (Line 1). Impedance magnitude loci show very different behaviour for the stable and unstable dynamics. Stable behaviour shows the impedance magnitude spends more time on the right-hand side of the *R-X* plane, but the unstable locus exhibits a massive journey on the left-hand side of the *R-X* plane.
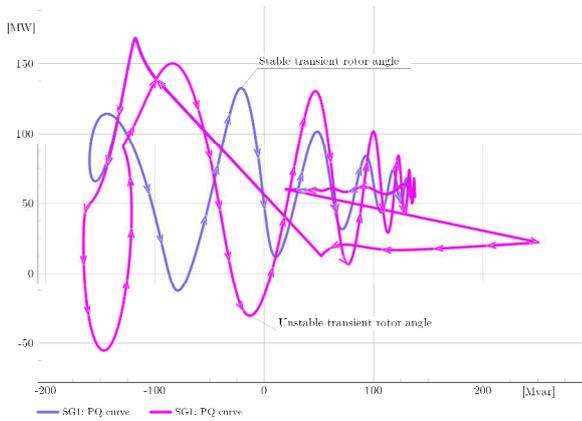
Fig. 8. Plot of active power versus reactive power (PQ plane) of SG1 during a transient rotor angle stability. Stable condition when fault is cleared at $t = 0.977$ sec and unstable at $t = 0.979$ sec.
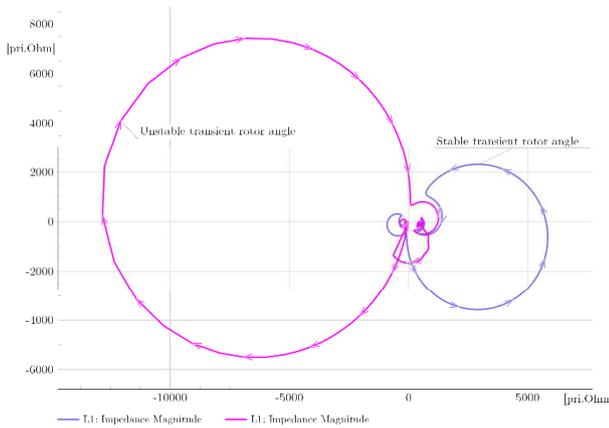
Fig. 9. Plot of resistance versus reactance (*RX*-plane) of the impedance |*Z*| 'seens' on Line 1. Stable condition when fault is cleared at $t < t_{CFCT} = 0.977$ sec and unstable at $t < t_{CFCT} = 0.979$ sec.

B. Assessing the critical clearing time of SynC

The dynamic performance of the SynC during and after a short circuit is very different when compared to the SG₁. The first clear difference between the synchronous machine and the power electronic converter is the transient overload capacity. While the synchronous generator can reach more than twice the rated current during a short circuit in a natural fashion (as shown in Fig. 10), the PEC equipped with a GFR controller is subject to a very strict current magnitude limitation time, especially during fault conditions.

The current limitation of a power electronic converter equipped with a SynC controller is clearly evident in Fig. 10. The virtual impedance controller is designed to calculate the real and reactive voltage drop across the virtual impedance (see (1), including a current limiter. However, the current limitation is fully enforced during the final output voltage calculation; the

current implementation used in this paper considers a current magnitude limitation of 1.2 pu. Fig. 10 shows how the current magnitude reaches 9.23 kA during the fault condition (stable and unstable conditions) but then following the clearing of the fault; the current is still at the limit during the voltage recovery period. The limited overcurrent period following the fault clearing is caused by the amount of reactive power required to recover the voltage during the post contingency condition. The SynC controller tries to mimic the dynamic performance of the synchronous machine; to do so, it follows a second-order linear differential equation to imitate the rotor angle and frequency of a fictitious synchronous generator, which is presented in (2). The model includes an acceleration time (T_{acel}) of the identical value of the SG₁ for comparative purposes. In this paper, the authors consider the fictitious rotor angle created by the SynC controller as the primary indicator to describe two possible operating conditions, the so-called stable transient rotor angle where the response no produces a phase jump. Using time-domain simulation, the authors identified that the maximum time the fault can be cleared without producing a phase jump to a negative angle was $t_{clear} = 4.0$ secs; this situation is depicted in Fig. 11.
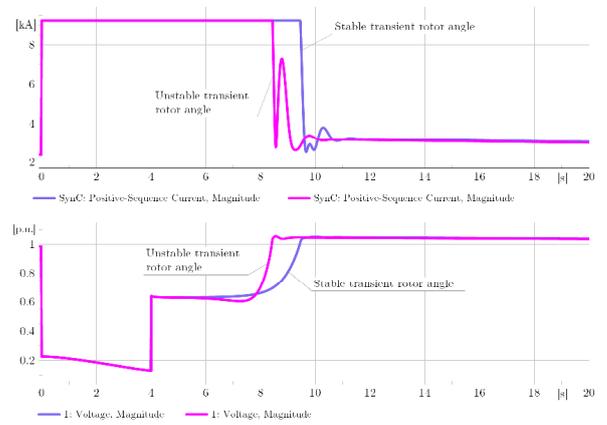
Fig. 10. Plot of current (|*I*|) and voltage (|*V*|) magnitude of SG1 during a transient rotor angle stability. Stable condition when fault is cleared at $t = 4.0$ sec and unstable at $t = 4.01$ sec.
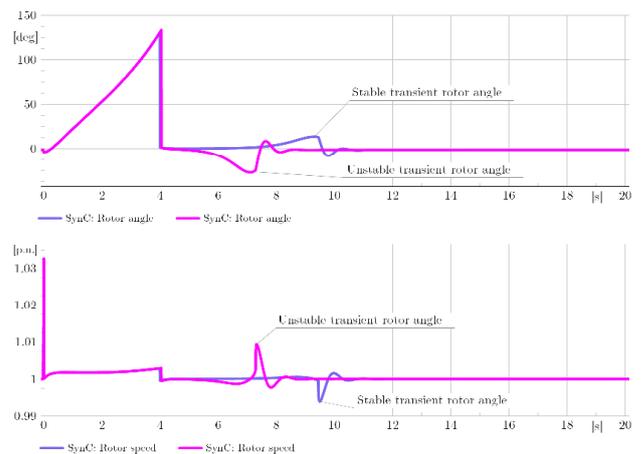
Fig. 11. Plot of rotor angle (θ_r) and speed (ω_r) of SG₁ during a transient rotor angle stability. Stable condition when fault is cleared at $t = 4.0$ sec and unstable at $t = 4.01$ sec.

Fig. 12 made clear the concept used in this paper for stable and unstable transient rotor angle; the stable trajectory of the active and reactive power involves both of them spending the majority of the trajectory inside the positive region of active power. However, an unstable condition made the trajectory spend the majority of the time in the negative P-semi-plane ($P<0$). A very interesting aspect of the PQ-trajectory is that plotting the stable and unstable conditions, the semicircle defining the locus of constant apparent power ($|S|=$ constant) is depicted. Fig. 13 shows the shows locus of the impedance magnitude ($|Z|$ in primary Ohms) measured at the terminal connected to ② of the faulted transmission line (Line 1) when compared to the one produced by the synchronous generator for similar conditions (stable and unstable), it results in evident dissimilarities between them. An unstable condition sends the RX trajectory to the negative reactance semi-plane ($X<0$), but the SynC controller provides a less distinctive trajectory.
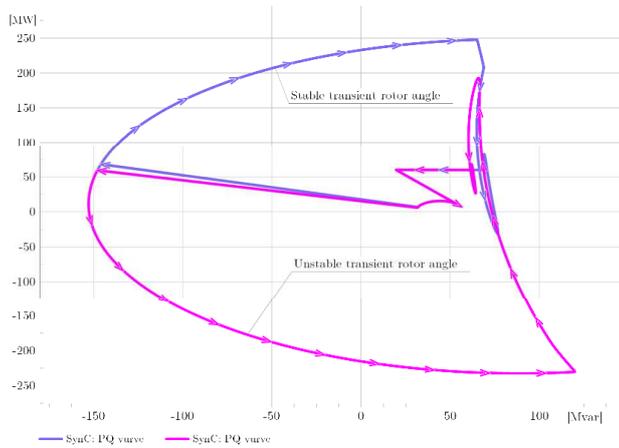
Fig. 12. Plot of active power versus reactive power (PQ-plane) of SG₁ during a transient rotor angle stability. Stable condition when fault is cleared at $t = 4.0$ sec and unstable at $t = 4.01$ sec.
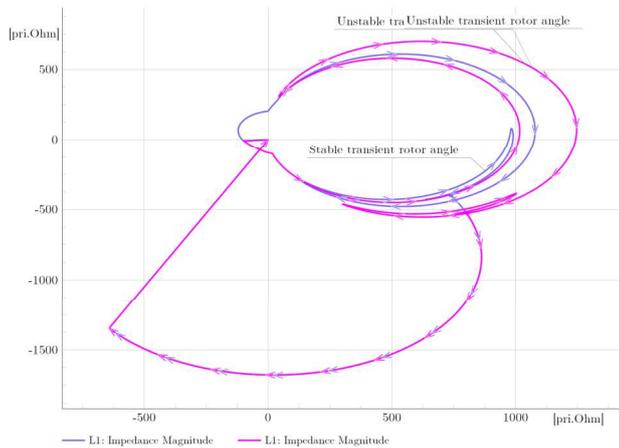
Fig. 13. Plot of active power versus reactive power (PQ-plane) of SynC during a transient rotor angle stability. Stable condition when fault is cleared at $t = 4.0$ sec and unstable at $t = 4.01$ sec.

V. CONCLUSIONS

This paper presents a comparative analysis (when possible between) IBG using synchronverter control technique and a traditional SG during transient stability conditions. This research is only a beginning point for characterising the performance of grid formation controller fault circumstances and their consequences on the electrical power system's transient stability. The simulations described in this research are straightforward, but they provide a glimpse into the future of power converter-dominated systems. Power converter-based systems with grid forming controllers outperform synchronous generators in terms of speed and behaviour.

REFERENCES

[1] Y. Rajbhandari *et al.*, "Load prioritisation technique to guarantee the continuous electric supply for essential loads in rural microgrids," *Int. J. Electr. Power Energy Syst.*, vol. 134, no. November 2020, p. 107398, Jan. 2022, doi: 10.1016/j.ijepes.2021.107398.

[2] A. Shrestha, B. Ghimire, and F. Gonzalez-Longatt, "A Bayesian Model to Forecast the Time Series Kinetic Energy Data for a Power System," *Energies*, vol. 14, no. 11, p. 3299, Jun. 2021, doi: 10.3390/en14113299.

[3] A. Shrestha and F. Gonzalez-Longatt, "Frequency Stability Issues and Research Opportunities in Converter Dominated Power System," *Energies*, vol. 14, no. 14, p. 4184, Jul. 2021, doi: 10.3390/en14144184.

[4] J.-M. Roldan-Fernandez, J. Serrano-Gonzalez, F. Gonzalez-Longatt, and M. Burgos-Payan, "Impact of Spanish Offshore Wind Generation in the Iberian Electricity Market: Potential Savings and Policy Implications," *Energies*, vol. 14, no. 15, p. 4481, Jul. 2021, doi: 10.3390/en14154481.

[5] M. N. Acosta, F. Gonzalez-Longatt, J. M. Roldan-Fernandez, and M. Burgos-Payan, "A Coordinated Control of Offshore Wind Power and BESS to Provide Power System Flexibility," *Energies*, vol. 14, no. 15, p. 4650, Jul. 2021, doi: 10.3390/en14154650.

[6] F. Gonzalez-Longatt, M. N. Acosta, H. R. Chamorro, and Jose Luis Rueda, "Power Converters Dominated Power Systems," in *Modelling and Simulation of Power Electronic Converter controlled Power Systems in PowerFactory*, First Edit., F. Gonzalez-Longatt and Jose Luis Rueda, Eds. Switzerland: Springer Nature Switzerland AG, 2021.

[7] D. Larrahondo, R. Moreno, H. R. Chamorro, and F. Gonzalez-Longatt, "Comparative Performance of Multi-Period ACOPF and Multi-Period DCOPF under High Integration of Wind Power," *Energies*, vol. 14, no. 15, p. 4540, Jul. 2021, doi: 10.3390/en14154540.

[8] H. R. Chamorro *et al.*, "Data-Driven Trajectory Prediction of Grid Power Frequency Based on Neural Models," *Electronics*, vol. 10, no. 2, p. 151, Jan. 2021, doi: 10.3390/electronics10020151.

[9] M. N. Acosta, F. Gonzalez-Longatt, D. Topić, and M. A. Andrade, "Optimal Microgrid–Interactive Reactive Power Management for Day–Ahead Operation," *Energies*, vol. 14, no. 5, p. 1275, Feb. 2021, doi: 10.3390/en14051275.

[10] F. S. Gorostiza and F. Gonzalez-Longatt, "Deep Reinforcement Learning-Based Controller for SOC Management of Multi-Electrical Energy Storage System," *IEEE Trans. Smart Grid*, pp. 1–1, 2020, doi: 10.1109/TSG.2020.2996274.

[11] "High Penetration of Power Electronic Interfaced Power Sources and the Potential Contribution of Grid Forming Converters European Network of Transmission System Operators for Electricity ENTSO-E Technical Group on High Penetration of Power Electronic Interfaced Power Sources." Accessed: Mar. 30, 2021. [Online]. Available: www.entsoe.eu.

[12] Australian Energy Market Operator, "Black System South Australia 28 September 2016," 2017. Accessed: Mar. 30, 2021. [Online]. Available: www.aemo.com.au.

[13] IEEFA, "Australia's Opportunity To Plan Ahead for a Secure Zero-Emissions Electricity Grid Towards Ending the Reliance on Inertia for Grid Stability," 2021.

[14] M. Habibullah, F. Gonzalez-Longatt, M. N. Acosta Montalvo, H. R. . Chamorro, J. L. Rueda, and P. Palensky, "On Short Circuit of Grid-Forming Converters Controllers: A glance of the Dynamic Behaviour," in *2021 IEEE PES Innovative Smart Grid Technologies Conference - Latin America (ISGT Latin America)*, Sep. 2021, pp. 1–5, doi:

10.1109/ISGTLatinAmerica52371.2021.9543017.

[15] National Grid, "System Operability Framework 2016," *UK Electr. Transm.*, no. November, pp. 68–72, 2016, Accessed: Mar. 30, 2021. [Online]. Available: www.nationalgrid.com/sof.

[16] N. Hatziargyriou *et al.*, "Stability definitions and characterisation of dynamic behavior in systems with high penetration of power electronic interfaced technologies," Dec. 2020. doi: 10.1109/JSYST.2015.2444893.

[17] R. Jadeja, A. Ved, T. Trivedi, and G. Khanduja, "Control of Power Electronic Converters in AC Microgrid," in *Power Systems*, vol. 27, no. 11, 2020, pp. 329–355.

[18] U. Tamrakar, D. Shrestha, M. Maharjan, B. Bhattarai, T. Hansen, and R. Tonkoski, "Virtual Inertia: Current Trends and Future Directions," *Appl. Sci.*, vol. 7, no. 7, p. 654, 2017, doi: 10.3390/app7070654.

[19] Q. C. Zhong and G. Weiss, "Synchronverters: Inverters that mimic synchronous generators," *IEEE Trans. Ind. Electron.*, vol. 58, no. 4, pp. 1259–1267, Apr. 2011, doi: 10.1109/TIE.2010.2048839.